Journal of The Electrochemical Society, **157** (12) H1148-H1152 (2010)
0013-4651/2010/157(12)/H1148/5/$28.00 © The Electrochemical Society

Interfacial Atomic Bonding Structure of Oxides on InAs(001)-(4 × 2) Surface

Jian Shen,[a,b,*,z] Wilhelm Melitz,[a,b] Sangyeob Lee,[b] Darby L. Feldwinn,[b] Ravi Droopad,[c,*] and Andrew C. Kummel[b,*]

[a]*Materials Science and Engineering Program and* [b]*Department of Chemistry and Biochemistry, University of California, San Diego, La Jolla, California 92093, USA*
[c]*Department of Physics, Texas State University, San Marcos, Texas 78666, USA*

Oxide monolayers and submonolayers formed by vapor deposition of In_2O and SiO oxides on InAs(001)-(4 × 2) were studied by scanning tunneling microscopy. At low coverage, In_2O molecules bond to the edges of the rows and most likely form new In–As bonds to the surface without any disruption of the clean surface structure. Annealing the In_2O/InAs(001)-(4 × 2) surface to 380°C results in the formation of flat ordered monolayer rectangular islands. The annealed In_2O no longer bonds with just the As atoms at the edge of row but also forms new O–In bonds in the trough. SiO chemisorption on InAs(001)-(4 × 2) is completely different than In_2O chemisorption. At room temperature, even at low coverage SiO adsorbates bond to themselves and form nanoclusters. For SiO/InA(001)-(4 × 2) postdeposition annealing does not disperse the nanoclusters into flat islands. Both In_2O and SiO depositions on the InAs(001)-(4 × 2) surface do not displace surface atoms during both room temperature deposition and postdeposition annealing.
 [DOI: 10.1149/1.3501053]

Manuscript received August 4, 2010. Published October 25, 2010. This was Paper 1495 presented at the Las Vegas, Nevada, Meeting of the Society, October 10–15, 2010.

The current silicon based integrated circuits (ICs) technologies have dominated the high-performance logic industry for decades. The success with the semiconductor IC industries lies in device downsizing: scaling. However, continuing the scaling is becoming increasingly difficult, and silicon transistor technology is rapidly approaching its physical limits. According to the 2008 updated International Technology Roadmap for Semiconductors,[1] to attain adequate drive current for highly scaled metal-oxide semiconductor field-effect transistors (MOSFETs), eventually other high transport channel materials (Ge and III–V) are needed for beyond 22 nm node generation so that semiconductor industries can continue keeping Moore's law.

Recently, extensive studies have been carried out on III–V compound semiconductors for potential channel materials of MOSFETs.[2-4] Several academic and industry groups have shown promising III–V MOSFETs results.[5-12] However, the interface between oxides and III–V semiconductors is not well understood. Forming electrically passive interfaces between the gate oxide and the channel[13] is still a major issue for the development of MOSFETs devices. Unlike hydrogen passivated silicon and SiO_2 interfaces ($D_{it} \sim 10^{10}$ eV^{-1} cm^{-2}),[14] oxide/III–V interfaces have large interfacial trap densities, D_{it} between 10^{12} and 10^{14} eV^{-1} cm^{-2},[15,16] so enhancement mode III–V MOSFETs devices require very high capacitance, even to counteract the lowest reported the interfacial trap densities. In order to obtain a fundamental understanding of surface passivation of III–V compound semiconductors, it is critical to investigate and understand surface morphological evolution and the oxide/semiconductor interface bonding at the atomic level in order to facilitate gate-oxide selection for III–V MOSFETs device and enable very aggressive oxide scaling.

InAs is an attractive channel material for high speed, low power MOSFET due to its very high effective electron mobility (~ 15 000 cm^2 V^{-1} s^{-1}) compared to Si (~ 300 cm^2 V^{-1} s^{-1}) at 300 K.[17] InAs FET results have shown that there is potential for high-performance InAs based MOSFET.[18,19] This report is focused upon the $c(8 \times 2)/(4 \times 2)$ surface since other surfaces such as As-rich (2 × 4) reconstruction readily undergoes oxygen induced displacement reactions.[20-23] Although InAs(001) (Ref. 24-26) have been the focus of many scanning tunneling microscopy (STM) studies, only one STM study has been performed on the bonding geometry of the oxide on the InAs(001) surface.[27]

To develop an atomic understanding of oxide morphologies on InAs(001)-$c(8 \times 2)/(4 \times 2)$, the bonding geometries of two different oxides In_2O and SiO on InAs(001)-$c(8 \times 2)/(4 \times 2)$ were investigated. STM was used to determine the exact interfacial bonding geometries of In_2O and SiO/InAs(001)-$c(8 \times 2)/(4 \times 2)$ after room temperature (RT) oxide deposition. In addition, the effects of postdeposition annealing (PDA) on oxide bonding sites were investigated. The results are focused on InAs, but the results are readily applied to InGaAs systems due to similar surface structure and oxide bonding geometry.[28]

Experimental and Computational Method

MBE was employed to grow 0.2 μm of 1 × 1018 cm^{-3} doped InAs layer on 500 μm thick InAs(001) substrates with 1 × 10^{18} cm^{-3} doping. Experiments were performed on both n-type and p-type wafers. The regrown wafers were capped in situ with a 50 nm protective arsenic cap. The wafers were transferred to a vacuum container for transporting to the STM chamber. Experiments were performed in two ultrahigh vacuum chamber systems with base pressures of 2 × 10^{-10} Torr. Each chamber was equipped with low energy electron diffraction (LEED) and either a Park Scientific room temperature or an Omicron variable temperature STM. The InAs(001)-$c(8 \times 2)/(4 \times 2)$ surface was prepared by thermal decapping method. Details concerning the decapping method used in this study have been discussed elsewhere.[28,29]

After the $c(8 \times 2)/(4 \times 2)$ surface reconstruction was verified by LEED, the sample was transferred to the STM chamber, where STM measurements were performed at room temperature. All of the STM measurements were carried out at RT using electrochemically etched tungsten tips. The InAs(001)-$c(8 \times 2)/(4 \times 2)$ clean surfaces could be observed with both filled and empty states STM. Subsequently, In_2O or SiO was deposited in the main chamber by evaporating sintered In_2O_3(s) (Aldrich Chem. Co.) or SiO(s) (Alfa Aesar) from a high temperature effusion cell (Applied EPI) contained in a differentially pumped chamber. In_2O_3(s) sublimates as In_2O(g) and O_2(g) at 1000–1025°C.[30] However, due to the low sticking probability of O_2 on group III-rich $c(8 \times 2)/(4 \times 2)$ surfaces,[31] the majority of the adsorbed species are In_2O. SiO(s) evaporates congruently as SiO(g) molecules at 950–975°C.[29]

* Electrochemical Society Active Member.
z E-mail: jimshen@ucsd.edu

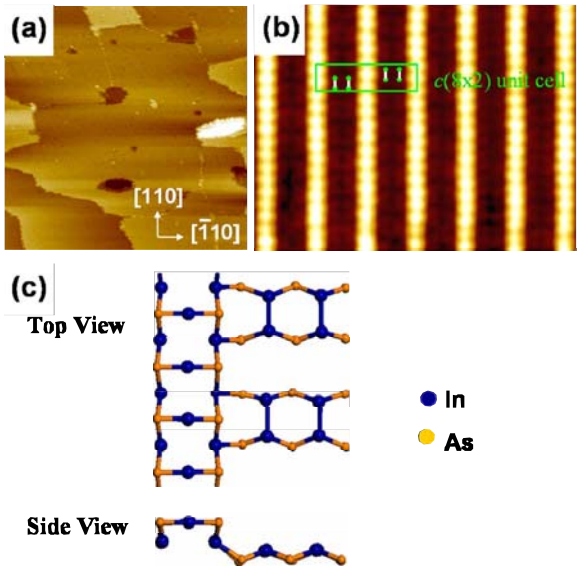

Figure 1. (Color online) Structure of clean InAs(001)-(4 × 2) at 300 K. (a) A filled state (Vs = −2 V, It = 0.2 nA, 2000 Å × 2000 Å) STM image obtained from the InAs(001)-(4 × 2) clean surface. (b) A high resolution filled state (Vs = −2 V, It = 0.2 nA, 100 Å × 85 Å) STM image obtained from the InAs(001)-(4 × 2) clean surface. (c) Ball-and-stick diagram of the InAs(001)-(4 × 2) reconstruction. The atomic InAs(001)-(4 × 2) reconstruction structure model has been discussed in Ref. 22. The green rectangle presents the unit cell of $c(8 \times 2)$. Note that In atoms on the row are undimerized, and the In row atoms have the same height as the As atoms at the edge of row.

During evaporation, the main chamber pressure is 2×10^{-7} and 5×10^{-9} Torr for In_2O and SiO, respectively.

Results and Discussion

In-rich InAs(001)-(4 × 2) can readily be prepared by decapping of As_2 capped InAs(001) wafers. A typical STM image of a clean InAs(001)-$c(8 \times 2)/(4 \times 2)$ surface prepared by decapping method can been seen in Fig. 1a. All STM images in this study were taken with a negative sample bias using the constant-current tunneling mode. The InAs(001)-(4 × 2) surface has a unit cell consisting of two undimerized group III atoms on the row and two group III homodimers in the trough. Details of the InAs(001)-(4 × 2) clean surface structure are discussed elsewhere.[26]

Indium monoxide (In_2O).— Once the surface structure of InAs(001)-(4 × 2) was characterized, the gate oxides were deposited to investigate the exact atomic bonding structures of gate-oxide/III–V interfaces. STM results showed that the initial deposited In_2O molecules bond to the edges of the rows and most likely form new In–As bonds to the surface without any disruption of the clean surface structure, shown in Fig. 2a. In filled state STM images, In_2O is imaged as a bright feature on the clean InAs(001)-(4 × 2) surface. Figure 2b shows a structural model illustrating the possible oxide bonding structure for room temperature deposition. Density function theory (DFT) results show that the binding energy is 0.84 eV/In_2O for InAs surface.[28] The binding energy[32] was calculated by subtracting the total energy of the most stable clean surface structure and gas phase oxide molecule from the total energy of the oxide/InAs complex: $E_{\text{bind}}^{\text{oxide/InAs}} = E^{\text{oxide/InAs}} - (E^{\text{InAs}} + E^{\text{oxide}})$, where $E_{\text{bind}}^{\text{oxide/InAs}}$ is the binding energy between oxide molecules and InAs surface, $E^{\text{oxide/InAs}}$ is the total energy of oxide deposited InAs double unit cell slab, E^{InAs} is the total energy of the clean InAs double unit cell slab, and E^{oxide} is the total energy of free oxide molecules.[28]

A height distribution analysis was performed to determine the room temperature growth mechanism. At medium coverage (~25% monolayer), the In_2O formed islands that are in the [110] direction, as shown in Fig. 2a. Prior to all the first layer bonding sites being occupied with oxides, distinct second layer growth is observed on

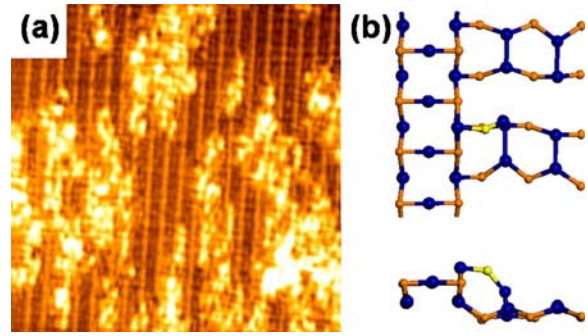

Figure 2. (Color online) Bonding of RT deposited In_2O/InAs(001)-(4 × 2). (a) A filled state (Vs = −1.5 V, It = 0.2 nA, 35 Å × 35 Å) STM image obtained from the InAs(001)-(4 × 2) surface with ~25% coverage of In_2O. (b) Possible atomic bonding structure diagrams of In_2O/InAs(001)-(4 × 2) surface along single In_2O chemisorption bonding sites with top view (upper) and side view (lower). Note that this image is taken in the Park Scientific RT-STM system.

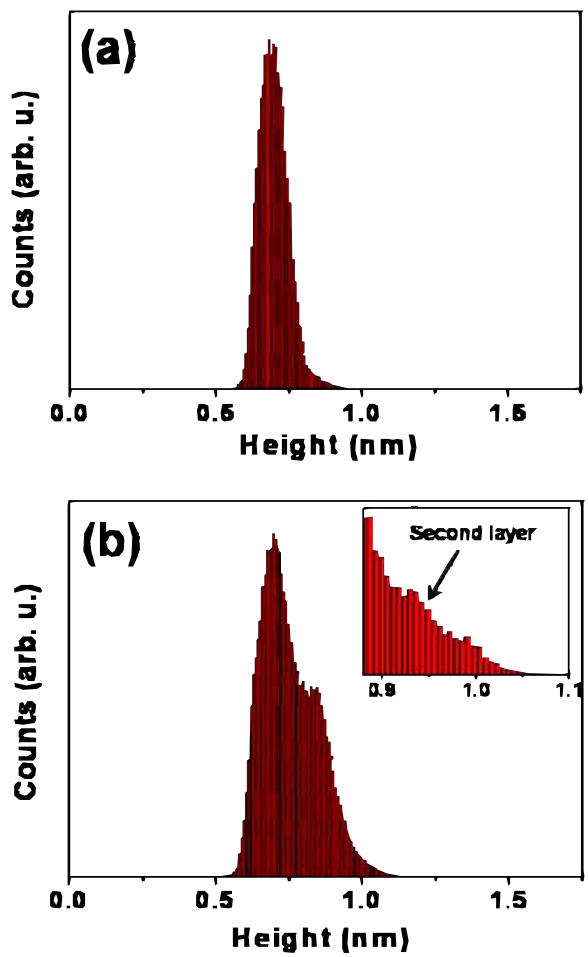

Figure 3. (Color online) Height analysis for RT deposition of In_2O/InAs(001)-(4 × 2). (a) Height distribution of only the oxide-free regions of the In_2O/InAs(001)-(4 × 2) surface in Fig. 2a. (b) Height distributions of the entire In_2O/InAs(001)-(4 × 2) surface in Fig. 2a. There are two position peaks corresponding to the clean surface region and the oxide covered surface region. The distance between two peaks is 1.5 Å. Inset in (a) is an expanded height distribution of In_2O deposited surface at the higher height region that reveals distinct second layer growth.

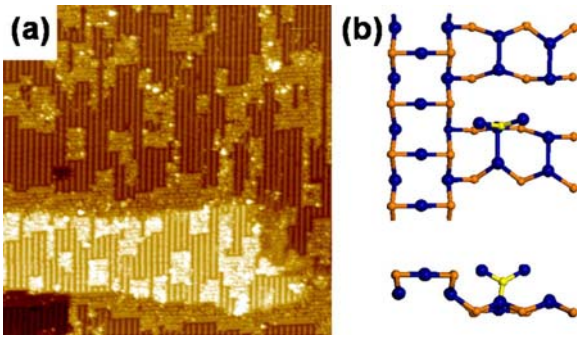

Figure 4. (Color online) Bonding of RT deposited In_2O/InAs(001)-(4 × 2) after a 380°C anneal. (a) A filled state (Vs = −2.5 V, It = 0.2 nA, 1000 Å × 1000 Å) STM image obtained from the InAs(001)-(4 × 2) surface. (b) Possible atomic bonding structure diagrams of annealed In_2O/InAs(001)-(4 × 2) surface along single In_2O chemisorption bonding sites with top view (upper) and side view (lower).

the oxide islands. Figure 3 shows In_2O height distribution for room temperature oxide deposition. For only clean surface region, there is height distribution peak near 7.0 Å, shown in Fig. 2a. For the whole surface, there is a bimodal height distribution shown in Fig. 3b with a lower position peak, which is identical to the clean region height distribution of the InAs(001)-c(8 × 2)/(4 × 2) surface. The higher

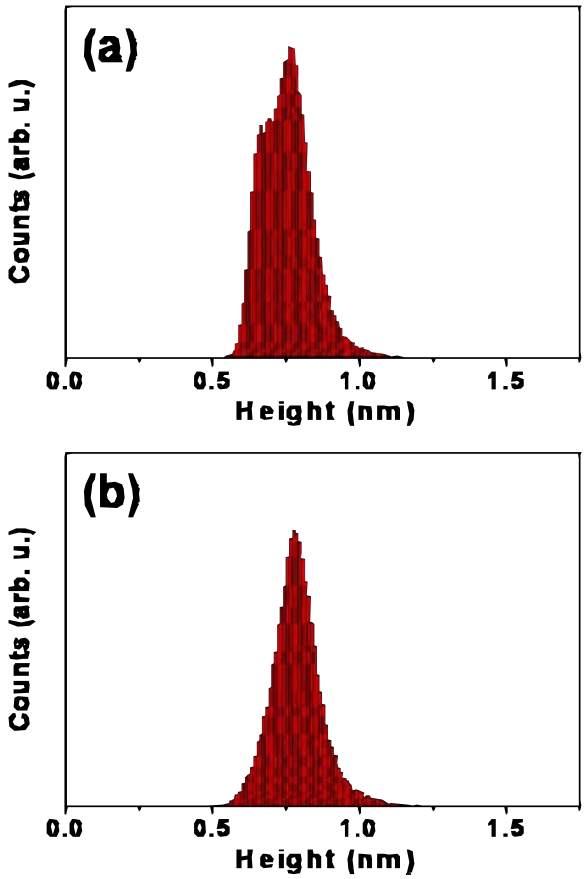

Figure 5. (Color online) Height analysis for RT deposition and 380°C annealing of In_2O/InAs(001)-(4 × 2). (a) Height distributions of In_2O deposited and annealed InAs(001)-(4 × 2) in Fig. 4a. (b) Height distribution of only the oxide covered regions of In_2O deposited and annealed InAs(001)-(4 × 2) in Fig. 4a. There are two position peaks corresponding to the clean surface region and the oxide covered surface region, respectively. The distance between the two peaks is 1.1 Å.

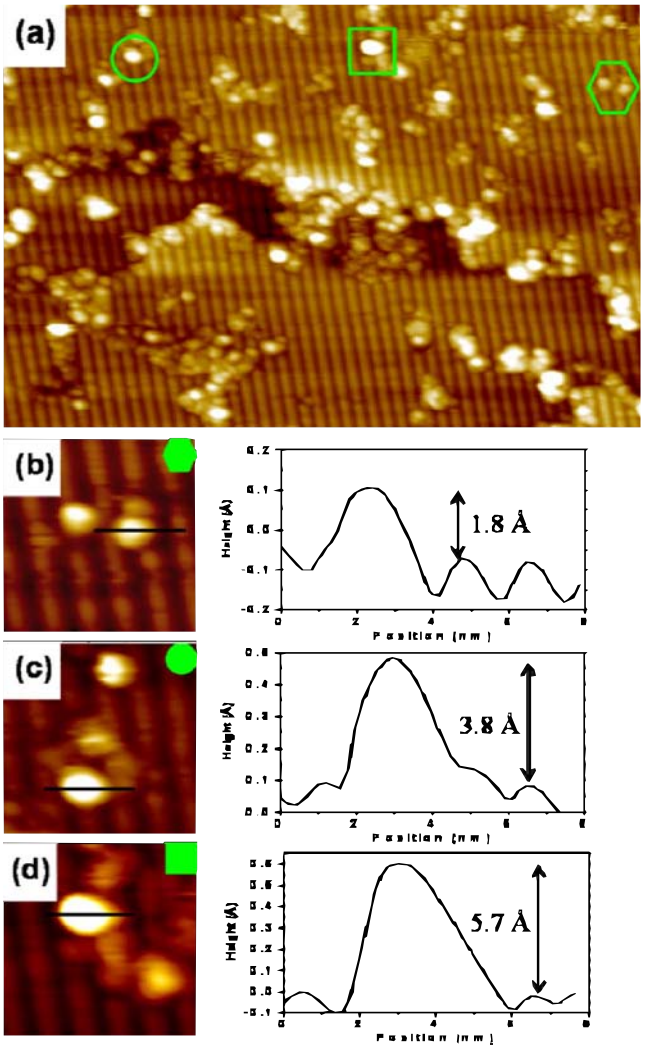

Figure 6. (Color online) STM image of the InAs(001)-(4 × 2) surface after low coverage SiO deposition (∼ 4% mL) at 300 K with PDA. (a) A filled state (Vs = −2.5 V, It = 0.2 nA, 80 Å × 55 Å) STM image obtained from SiO deposited InAs(001)-(4 × 2) surface. Three magnified STM images illustrate three different heights with corresponding geometric symbols, and line scan corresponding to the black line on the STM image revealing that SiO adsorbates bond themselves and form nanoclusters: (b) hexagon, 1.8 Å height with 12 Å × 12 Å size; (c) circle, 3.8 Å height with 16 Å × 12 Å size; and (d) square, 5.7 Å height with 20 Å × 16 Å size. Note that a single SiO molecule's size is about 4 Å × 4 Å according to Ref. 29.

position peak corresponds to the oxide covered surface. The 1.5 Å height difference between the oxide and clean surface is consistent with single monolayer growth consistent with the line scan analysis performed on the Fig. 2 STM image. Inset in Fig. 3b is expanded height distribution of In_2O deposited surface at the higher height region that is consistent with the second layer oxide growth on the oxide islands. The first and second layers of oxide have the distinct heights corresponding to distinct layers of oxide. However, the second and subsequent oxide layers appear to be amorphous since these oxides do not form ordered structures.

To form more ordered oxide structures, the effect of annealing In_2O/InAs(001)-c(8 × 2)/(4 × 2) was studied. Postdeposition annealing induced the oxide to spread out. As shown in Fig. 4, the 380°C annealed samples were more ordered with respect to both island shape and the structure within the islands consistent with the lowest energy structure being an ordered first monolayer of oxides. The ordered structures contained oxide in the troughs with rows in the $[\bar{1}10]$ direction. Comparisons of oxide height distributions be-

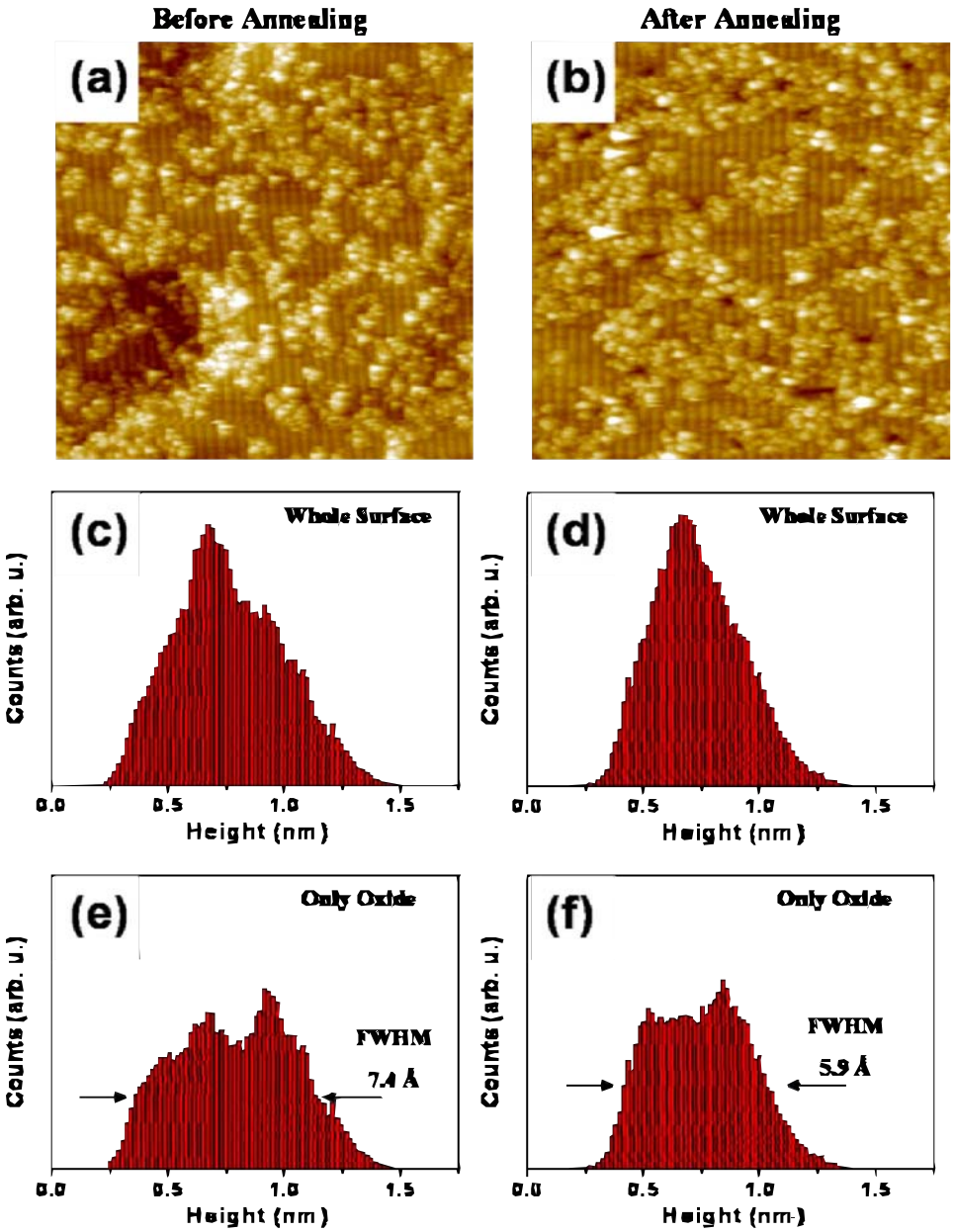

Figure 7. (Color online) STM images and the height distributions of the InAs(001)-(4 × 2) surface after 35% coverage of SiO deposition. Filled state (Vs = −2.5 V, It = 0.2 nA, 700 Å × 700 Å) STM images obtained from SiO deposited InAs(001)-(4 × 2) surface (a) without and (b) with postdeposition annealing (PDA) at 380°C. (c) Height distribution of the entire Si_2O/InAs(001)-(4 × 2) surface without PDA shown in Fig. 7a. (d) Height distribution of the entire Si_2O/InAs(001)-(4 × 2) surface with PDA shown in Fig. 7b. (e) Height distribution of the oxide covered regions of SiO/InAs(001)-(4 × 2) without PDA. (e) Height distribution of the oxide covered regions of SiO/InAs(001)-(4 × 2) with PDA.

fore and after annealing show that the oxide height is reduced from 1.5 to 1.1 Å, shown in Fig. 5a. For the oxide covered regions of the surface, there is a Gaussian height distribution shown in Fig. 5b with a full width at half maximum (fwhm) of only 1.8 Å, which is consistent with the formation of flat monolayer island structures with the 1.8 Å corrugation being primarily due to the apparent STM height difference between the indium and oxygen atoms in In_2O adsorbates. Most importantly, for both room temperature deposition and postdeposition annealing, the In_2O adsorbates never cause the displacements of any surface atoms on the InAs(001)-c(8 × 2)/(4 × 2) surface; if the annealing temperature is raised above 450°C using cyclic annealing,[29] the In_2O molecules completely desorb, leaving behind the clean (4 × 2) surface.[28] The 380°C annealing induced formation of dense flat square monoatomically tall islands, indicating that a new bonding geometry forms after postdeposition annealing. DFT simulations show that the annealed In_2O no longer bonds with just the As atoms at the edge of row but also forms new O–In bonds in the trough, shown in Fig. 4b. For In_2O, In_2O–In trough sites are more stable than In–O–In–As edge sites by about ~0.77 eV/In_2O.[28]

Silicon monoxide (SiO).— Figure 6 shows an STM image of the InAs(001)-(4 × 2) surface after low coverage SiO deposition (~4% ML) at 300 K with PDA. The bright features on the surface are SiO molecules bonding with the InAs(001)-(4 × 2) substrate; some of the SiO bond to the rows and some of the SiO bond in the troughs. Magnified STM images show that there are three distinct types of bright features presented on the SiO/InAs(001)-(4 × 2) surface, which have been denoted by a hexagon, a circle, and a square. These bright sites can be clearly differentiated by line scan analysis. The results show that these bright sites represent heights of three different oxide layers. The hexagon (Fig. 6b) is found to image as 1.8 Å above the surface row. This height represents monolayer height since it is close to the height of a single SiO molecule on GaAs(001)-(2 × 4) surface.[29] The circle (Fig. 6c) is found to image as 3.8 Å above the surface row, indicating two layer SiO molecules on surface. The square (Fig. 6d) is found to image as 5.7 Å above the surface row, indicating three layer SiO molecules on surface. These bright features are consistent with the higher self-binding energy of SiO molecules to form multilayer structures on InAs(001)-(4 × 2).[33]

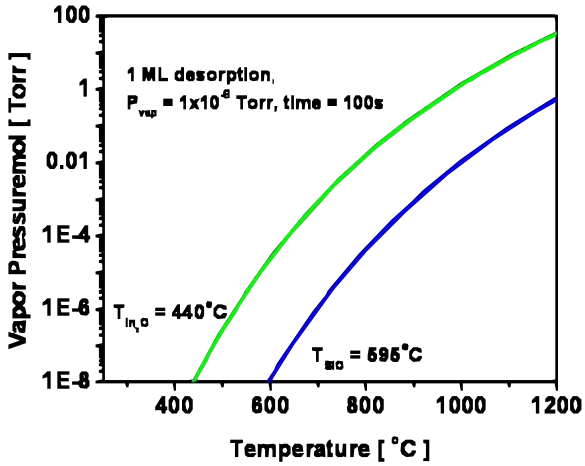

Figure 8. (Color online) The vapor pressure vs temperature for In_2O and SiO.

At 35% coverage of SiO deposited on the InAs(001)-(4 × 2) surface at room temperature, there is no ordered oxide structure formation. SiO molecules bond to themselves and form nanoclusters shown in Fig. 7a. The bonding configuration is nearly identical when the SiO/InAs sample was annealed to 380°C (Fig. 7b). Height distribution analyses were performed on SiO deposited InAs(001)-(4 × 2) surface without and with PDA at 380°C. As shown in Fig. 7c, for the whole surface without PDA, SiO deposited InAs(001)-(4 × 2) has a broad height distribution. For SiO/InAs(001)-(4 × 2) shown in Fig. 7c, there is a lower position peak (~7 Å height) which is the clean region of the InAs(001)-(4 × 2) surface. If only the oxide covered surface is included in the height distribution analysis, the results (Fig. 7e) show that the SiO/InAs(001)-(4 × 2) surface has much broader oxide height distribution (fwhm ~7.4 Å) which is 3.7× as large as the height distribution for the oxide covered regions of In_2O/InAs(001)-(4 × 2) (fwhm ~2 Å) shown in Fig. 3. After PDA at 380°C, the height distribution becomes smoother, consistent with the surface becoming slightly flatter. However, after PDA the oxide covered regions of SiO/InAs(001)-(4 × 2) have an fwhm of 5.9 Å, which is still 3× fwhm of the oxide covered regions for postdeposition annealed In_2O/InAs(001)-(4 × 2) (fwhm ~1.8 Å). This height distribution analysis is consistent with formation of nanoclusters for SiO deposited InAs surface. Further analysis of the SiO/InAs(001)-(4 × 2) surface after PDA shows no bright displaced As atoms nor dark oxygen sites. The common feature for both In_2O and SiO depositions on the InAs(001)-(4 × 2) surface is that oxides do not displace surface atoms during both room temperature deposition and postdeposition annealing. After oxide deposition, the InAs(001) surface retain the (4 × 2) reconstruction, even within a few angstroms of the adsorbates.

The experimental results show that In_2O molecules completely desorb at 450°C, leaving behind the clean (4 × 2) surface,[28] and SiO molecules remain on the surface even at 530°C (not shown). The temperatures above 530°C were not tried due to the heating limitations of the manipulator. Literature results show that for pure substances (not InAs chemisorbates) SiO has higher sublimation energy than In_2O (ΔH: SiO 3.3 eV versus In_2O 2.6 eV).[33] It is hypothesized that the lower self-binding energy allows In_2O to form monolayer flat ordered islands, while the higher self-binding energy induces SiO to form multilayer disorder amorphous structures on InAs(001)-(4 × 2). Figure 8 shows the vapor pressure for In_2O and SiO versus the temperature according to experimental data of Ref. 33-35. To desorb 1 ML of In_2O and SiO oxide from themselves (for example, 10^{-8} Torr vapor pressure for 100 s), the oxide temperature should be 440°C for In_2O and 595°C for SiO, which is consistent with the experimental results.

Conclusion

The bonding geometries of two different oxides In_2O and SiO on InAs(001)-c(8 × 2)/(4 × 2) were investigated using STM. The results show the completely different bonding geometries. In_2O molecules initially bond with As atoms at the edge of the row. After postdeposition annealing, In_2O molecules bond with the trough In atoms to form new O–In bonding sites. In_2O oxide forms dense flat monolayer tall island structures on the InAs(001)-c(8 × 2)/(4 × 2) surface. Conversely, SiO molecules have higher self-binding energy so that they bond themselves and form nanoclusters on the InAs(001)-c(8 × 2)/(4 × 2) surface. In_2O and SiO depositions on the InAs(001)-c(8 × 2)/(4 × 2) surface do not displace surface atoms during both room temperature deposition and postdeposition annealing.

Acknowledgments

The authors thank M. Passlack for the valuable discussions and N. M. Santagata for initial work. J. Shen is grateful for the support of Intel Foundation PhD Fellowship. This work was supported by SRC-NCRC-1437.003 and the FCRP-MSD-887.011.

References

1. International Technology Roadmap for Semiconductors (2008), http://www.itrs.net/Links/2008ITRS/Home2008.htm, last accessed Oct 18, 2010.
2. F. Ren, et al., *IEEE Electron Device Lett.*, **19**, 309 (1998).
3. P. D. Ye, et al., *Appl. Phys. Lett.*, **83**, 180 (2003).
4. R. Chau, S. Datta, M. Doczy, B. Doyle, J. Jin, J. Kavalieros, A. Majumdar, M. Metz, and M. Radosavljevic, *IEEE Trans. Nanotechnol.*, **4**, 153 (2005).
5. Y. N. Sun, E. W. Kiewra, J. P. de Souza, J. J. Bucchignano, K. E. Fogel, D. K. Sadana, and G. G. Shahidi, *IEEE Electron Device Lett.*, **30**, 5 (2009).
6. R. J. W. Hill, et al., *IEEE Electron Device Lett.*, **28**, 1080 (2007).
7. T. D. Lin, H. C. Chiu, P. Chang, L. T. Tung, C. P. Chen, M. Hong, J. Kwo, W. Tsai, and Y. C. Wang, *Appl. Phys. Lett.*, **93**, 033516 (2008).
8. A. M. Sonnet, C. L. Hinkle, M. N. Jivani, R. A. Chapman, G. P. Pollack, R. M. Wallace, and E. M. Vogel, *Appl. Phys. Lett.*, **93**, 122109 (2008).
9. Y. Xuan, Y. Q. Wu, and P. D. Ye, *IEEE Electron Device Lett.*, **29**, 294 (2008).
10. Y. Q. Wu, R. S. Wang, T. Shen, J. J. Gu, and P. D. Ye, *IEDM Tech. Dig.*, **2009**, 331.
11. Y. Q. Wu, M. Xu, R. Wang, O. Koybasi, and P. D. Ye, *IEDM Tech. Dig.*, **2009**, 323.
12. M. Radosavljevic, et al., *IEDM Tech. Dig.*, **2009**, 319.
13. M. J. Hale, S. I. Yi, J. Z. Sexton, A. C. Kummel, and M. Passlack, *J. Chem. Phys.*, **119**, 6719 (2003).
14. S. Iwata and A. Ishizaka, *J. Appl. Phys.*, **79**, 6653 (1996).
15. Y. Xuan, Y. Q. Wu, H. C. Lin, T. Shen, and P. D. Ye, *IEEE Electron Device Lett.*, **28**, 935 (2007).
16. N. Goel, P. Majhi, C. O. Chui, W. Tsai, D. Choi, and J. S. Harris, *Appl. Phys. Lett.*, **89**, 163517 (2006).
17. R. F. Service, *Science*, **323**, 1000 (2009).
18. N. Li, E. S. Harmon, J. Hyland, D. B. Salzman, T. P. Ma, Y. Xuan, and P. D. Ye, *Appl. Phys. Lett.*, **92**, 143507 (2008).
19. T. Bryllert, L. E. Wernersson, L. E. Froberg, and L. Samuelson, *IEEE Electron Device Lett.*, **27**, 323 (2006).
20. P. Kruse, J. G. McLean, and A. C. Kummel, *J. Chem. Phys.*, **113**, 9217 (2000).
21. P. Kruse, J. G. McLean, and A. C. Kummel, *J. Chem. Phys.*, **113**, 9224 (2000).
22. S. I. Yi, P. Kruse, M. Hale, and A. C. Kummel, *J. Chem. Phys.*, **114**, 3215 (2001).
23. D. L. Winn, M. J. Hale, T. J. Grassman, J. Z. Sexton, and A. C. Kummel, *J. Chem. Phys.*, **127**, 134705 (2007).
24. C. Kendrick, G. LeLay, and A. Kahn, *Phys. Rev. B*, **54**, 17877 (1996).
25. S. Ohkouchiand N. Ikoma, *Jpn. J. Appl. Phys., Part 1*, **33**, 3710 (1994).
26. D. L. Feldwinn, J. B. Clemens, J. Shen, S. R. Bishop, T. J. Grassman, A. C. Kummel, R. Droopad, and M. Passlack, *Surf. Sci.*, **603**, 3321 (2009).
27. J. B. Clemens, E. A. Chagarov, M. Holland, R. Droopad, J. Shen, and A. C. Kummel, *J. Chem. Phys.*, In press. [DOI: 10.1063/1.3487737]
28. J. Shen, E. A. Chagarov, D. L. Feldwinn, W. Melitz, N. M. Santagata, A. C. Kummel, and R. Droopad, *J. Chem. Phys.*, In press. [DOI: 10.1063/1.3497040]
29. D. L. Winn, M. J. Hale, T. J. Grassman, A. C. Kummel, R. Droopad, and M. Passlack, *J. Chem. Phys.*, **126**, 084703 (2007).
30. M. J. Hale, J. Z. Sexton, D. L. Winn, A. C. Kummel, M. Erbudak, and M. Passlack, *J. Chem. Phys.*, **120**, 5745 (2004).
31. J. B. Clemens, S. R. Bishop, D. L. Feldwinn, R. Droopad, and A. C. Kummel, *Surf. Sci.*, **603**, 2230 (2009).
32. S. M. Lee, S. H. Lee, and M. Scheffler, *Phys. Rev. B*, **69**, 125317 (2004).
33. J. Valderrama-n and K. T. Jacob, *Thermochim. Acta*, **21**, 215 (1977).
34. S. M. Schnurre, J. Grobner, and R. Schmid-Fetzer, *J. Non-Cryst. Solids*, **336**, 1 (2004).
35. R. D. Srivastava and M. Farber, *Chem. Rev. (Washington, D.C.)*, **78**, 627 (1978).